Loss-induced suppression, revival, and switch of photon blockade

Yunlan Zuo [1], Ran Huang [2,*], Le-Man Kuang [1,3,†], Xun-Wei Xu [1,‡] and Hui Jing [1,3,§]

[1]*Key Laboratory of Low-Dimensional Quantum Structures and Quantum Control of Ministry of Education, Department of Physics and Synergetic Innovation Center for Quantum Effects and Applications, Hunan Normal University, Changsha 410081, China*

[2]*Theoretical Quantum Physics Laboratory, RIKEN Cluster for Pioneering Research, Wako-shi, Saitama 351-0198, Japan*

[3]*Synergetic Innovation Academy for Quantum Science and Technology, Zhengzhou University of Light Industry, Zhengzhou 450002, China*

Loss-induced transparency (LIT), featuring the revival of optical intensity by adding loss, has been demonstrated in classical optics. However, a fundamental question has remained unexplored, i.e., during the process of LIT, whether quantum correlations of the photons can also be revived or even tuned by increasing the loss. Here we find that, accompanying classical LIT in a nonlinear optical-molecule system, a purely quantum effect as photon blockade (PB) indeed can be revived with the help of loss. In particular, a quantum critical point emerges in the system: below the point, adding loss leads to the suppression of optical intensity and its correlations; in contrast, by surpassing the point, PB is revived and enhanced with more losses. Also, a quantum switch between single-PB and two-PB can be realized by simply tuning the loss. Our work provides a counterintuitive strategy to engineer quantum devices in a practical lossy environment.

I. INTRODUCTION

Loss is ubiquitous in nature, which is usually regarded as harmful and undesirable in making and operating quantum devices. Very recently, loss has been found to play an unconventional role in non-Hermitian physics [1–3], such as loss-induced transparency (LIT) [4,5], loss-induced lasing revival [6], and loss-induced nonreciprocity [7,8]. These pioneering works, however, mainly focused on the classical regime, i.e., studying loss-tuned optical intensity, instead of the quantum correlation of light. As a further step, understanding the role of loss in engineering purely quantum effects not only facilitates the development of open quantum theories, but also provides a practical way to fabricate loss-controlled quantum devices inaccessible by conventional ways and allows exploring their applications in quantum technology.

In this work, we show how to engineer a purely quantum effect, i.e., photon blockade (PB), with the help of loss. PB has been demonstrated in diverse systems ranging from cavity QED [9–12] to superconducting circuits [13–15] and cavity-free devices [16]. PB provides a unique way not only to make important quantum devices [17–30], such as single-photon turnstiles [31], quantum routers [32], and quantum circulators [33], but also to explore the fundamental issues of quantum many-body physics [34–41]. To date, the main approaches for realizing PB are nonlinearity-induced anharmonic eigenenergy [9–11,14–16,42–44], and destructive interference between different modes [12,13,45–50]. Generically, the loss should be smaller than the strength of nonlinearity or the coupling of different modes since it is

regarded as limiting the efficiency or functionalities of PB devices.

Here we show that PB or the nonclassical correlations of photons can be suppressed and revived by adding loss in an optical compound system, accompanying the classical LIT. In the pioneering experiments on LIT [4,6], the revival of classical optical transmission is attributed to an exceptional point (EP), featuring the coalescence of both the complex eigenvalues and their corresponding eigenstates [51]. However, we find that, for the quantum revival of PB, not only does the EP-induced mode coalescence, but also the breakdown of the two-photon resonance is required. More interestingly, different types of quantum correlations can emerge in the revived light by merely increasing the loss (via placing an external nanotip near the optical resonator), resulting in a loss-tuned quantum switch between single-PB and two-PB. Our work drives the field of loss-induced effects into the purely quantum regime, where it becomes promising to study various quantum effects with lossy synthetic materials [8,52] or topological structures [53,54], as well as to build loss-tuned single-photon devices for quantum engineering [55–61].

II. MODEL AND METHOD

We consider an optical Kerr resonator ($\mu R1$) directly coupled to a linear resonator ($\mu R2$) with the coupling strength J [Fig. 1(a)], which can be described by ($\hbar = 1$):

$$\hat{H} = \hat{H}_i - i\frac{\gamma_1'}{2}\hat{a}_1^\dagger \hat{a}_1 - i\frac{\gamma_2'}{2}\hat{a}_2^\dagger \hat{a}_2,$$

$$\hat{H}_i = \sum_{j=1,2} \omega_c \hat{a}_j^\dagger \hat{a}_j + \hat{H}_{\text{int}}, \qquad (1)$$

$$\hat{H}_{\text{int}} = \chi \hat{a}_1^\dagger \hat{a}_1^\dagger \hat{a}_1 \hat{a}_1 + J(\hat{a}_1^\dagger \hat{a}_2 + \hat{a}_2^\dagger \hat{a}_1),$$

where $\hat{a}_{j=1,2}$ are the optical modes with resonance frequency ω_c, and $\chi = 3\hbar\omega_c^2\chi^{(3)}/(4\varepsilon_0\varepsilon_r^2 V_{\text{eff}})$ is the Kerr parameter with

*ran.huang@riken.jp
†lmkuang@hunnu.edu.cn
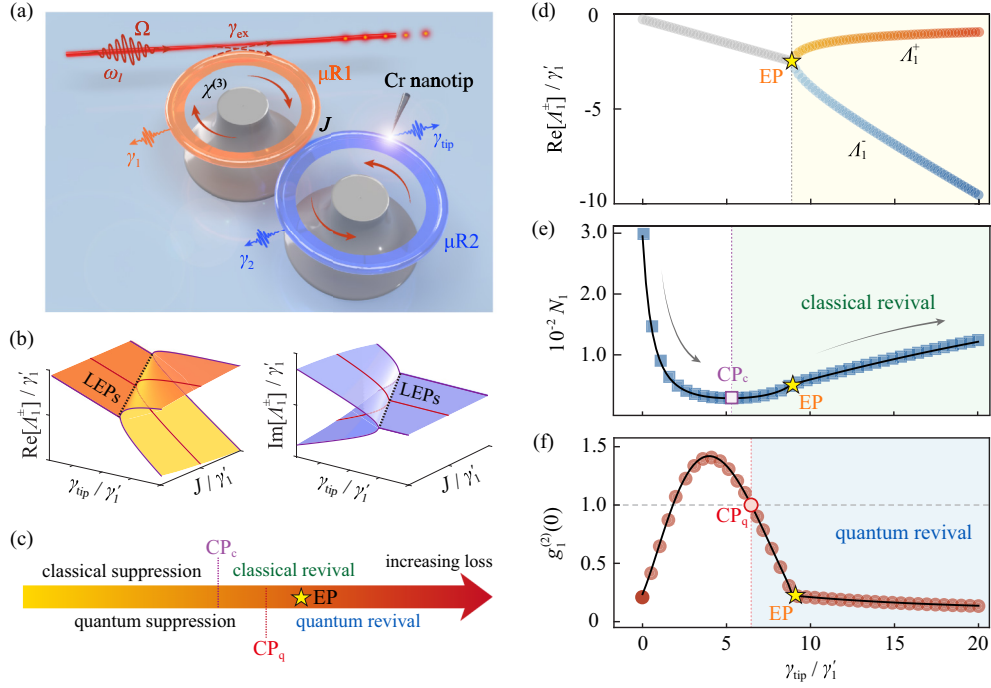‡davidxu0816@163.com
§jinghui73@foxmail.com

FIG. 1. The suppression and revival of quantum correlations in loss-induced transparency. (a) A whispering-gallery-mode resonator $\mu R1$ with Kerr-type nonlinearity $\chi^{(3)}$ coupled to a linear optical cavity $\mu R2$ with additional loss γ_{tip} induced by a Cr-coated nanotip, where J is the coupling strength between $\mu R1$ and $\mu R2$. (b) The Liouvillian exceptional points (LEPs, black dashed line) are shown in the eigenspectra $\Lambda_1^{\pm}$ of the system's Liouvillian. The red solid curves indicate the case of $J/\gamma_1' = 2$. (c) The suppression and revival in quantum correlation $g_1^{(2)}(0)$ (classical photon number N_1) are revealed by increasing loss before and beyond the quantum (classical) critical point CP_q (CP_c), respectively. (d) The real parts of $\Lambda_1^{\pm}$ versus γ_{tip} for $J/\gamma_1' = 2$. (e) The photon number N_1 and (f) quantum correlation $g_1^{(2)}(0)$ versus γ_{tip}, where markers (squares, circles) and black lines are analytical and numerical solutions, respectively. The parameters are given in the main text.

vacuum (relative) permittivity ε_0 (ε_r), nonlinear susceptibility $\chi^{(3)}$, and mode volume V_{eff}. In addition to nonlinear materials [62–66], Kerr-type nonlinearity can also be achieved in cavity or circuit QED systems [9,67,68], cavity-free systems [69], as well as optomechanical [18,70,71] or magnon devices [72,73].

The intrinsic losses of the two resonators are $\gamma_{j=1,2}$. The total loss of $\mu R1$ is given by $\gamma_1' = \gamma_1 + \gamma_{\text{ex}}$, where γ_{ex} is the loss induced by the coupling between $\mu R1$ and the fiber taper. An additional loss γ_{tip} is introduced on $\mu R2$ by a chromium (Cr) coated silica-nanofiber tip, featuring strong absorption in the 1550-nm band [6]. The strength of γ_{tip} can be increased by enlarging the volume of the nanotip within the cavity mode field, leading to a linewidth broadening without observable change in resonance frequency [6]. The total loss of $\mu R2$ is given by $\gamma_2' = \gamma_2 + \gamma_{\text{tip}}$.

Our system is identified as a passive parity-time symmetric system [3,74], where EPs exist in our system [Figs. 1(b) to 1(d)]; leading to the LIT effects [4–6]. As shown in Figs. 1(c) and 1(e), with an EP, increasing loss leads to classical suppression and revival of the mean-photon number $N_1 = \langle \hat{a}_1^{\dagger} \hat{a}_1 \rangle$, where the critical point with the minimum of N_1 is referred to as classical critical point (CP_c) between these two processes.

The quantum features of the light can be characterized by the second-order correlation function $g_1^{(2)}(0)$:

$$g_1^{(2)}(0) = \frac{\langle \hat{a}_1^{\dagger 2} \hat{a}_1^2 \rangle}{\langle \hat{a}_1^{\dagger} \hat{a}_1 \rangle^2}, \qquad (2)$$

with

$$g_1^{(2)}(0) \begin{cases} >1 & \text{super-Poissonian (bunching)}, \\ <1 & \text{sub-Poissonian (antibunching)}, \end{cases}$$

and $g_1^{(2)}(0) \to 0$ indicates a full single-PB. The quantum revival of single-PB can be considered as the transition of the quantum correlation from super-Poissonian (bunching) to sub-Poissonian (antibunching) [Figs. 1(c) and 1(f)]. Thus, we refer to the point with $g_1^{(2)}(0) = 1$ as the quantum critical point (CP_q).

We study the eigenenergy spectrum of this system by considering the effects of loss. The eigenstates of one or two excitations, i.e., $|\psi_1^{\pm}\rangle$ or $|\psi_2^{\pm,0}\rangle$, are the superposition states of the Fock state $|m, n\rangle$ with m photons in $\mu R1$ and n photons in $\mu R2$ (see details in Appendix A).

The complex eigenvalues of the one excitation are found as

$$\lambda_1^{\pm} = -i\Gamma + \omega_c \pm \sqrt{J^2 - \beta^2}, \qquad (3)$$

whose real and imaginary parts indicate the eigenfrequencies $\omega_1^{\pm}$ and the linewidths $\kappa_1^{\pm}$, respectively. Here, $\Gamma = (\gamma_1' + \gamma_2')/4$ and $\beta = (\gamma_2' - \gamma_1')/4$ quantify the total loss and the loss contrast of the system, respectively. The Hamiltonian EPs (HEPs) are defined as the spectral degeneracies of the non-Hermitian Hamiltonian [51], which emerge for $\lambda_1^+ = \lambda_1^-$
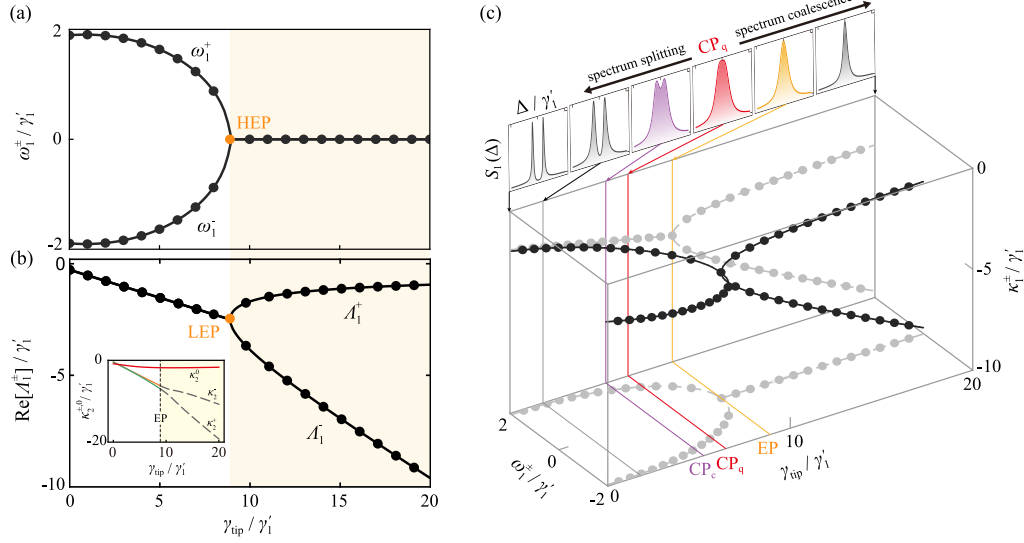
FIG. 2. (a) The eigenfrequencies $\omega_1^\pm$ as functions of γ_{tip}. (b) The real parts of the eigenvalues $\Lambda_1^\pm$ versus γ_{tip}. The inset shows the evolution of the linewidths $\kappa_2^{\pm,0}$ as a function of γ_{tip}. (c) The evolution of the excitation spectrum $S_1(\Delta)$ and eigenvalues versus γ_{tip}. The $S_1(\Delta)$ shows the spectrum splitting and spectrum coalescence. The parameters are the same as those in Fig. 1

[Figs. 2(a) and 2(c)], i.e.,

$$\gamma_{\text{tip}}^{\text{EP}} = 4J + \gamma_1' - \gamma_2. \tag{4}$$

For the two-excitations case, the frequencies $\omega_2^{+,0}$ and linewidths $\kappa_2^{+,0}$ are defined by the real and imaginary parts of the eigenvalues $\lambda_2^{+,0}$, respectively, i.e.,

$$\omega_2^{+,0} = \text{Re}[\lambda_2^{+,0}], \quad \kappa_2^{+,0} = \text{Im}[\lambda_2^{+,0}]. \tag{5}$$

By increasing γ_{tip}, the linewidths $\kappa_2^\pm$ coalesce before EP and split in the vicinity of EP [the inset of Fig. 2(b)].

Hamiltonian EPs do not take into account the quantum noise associated with quantum jumps. For a fully quantum picture, we consider the system's Liouvillian superoperator $\mathcal{L}$, which includes the effect of quantum jumps [75]. This can be done using the Lindblad master-equation approach, and the Liouvillian superoperator $\mathcal{L}$ is given by [75]

$$\mathcal{L}\hat{\rho} = -i[\hat{H}_i, \hat{\rho}] + \sum_{j=1,2} \mathcal{D}(\hat{\rho}, \hat{A}_j), \tag{6}$$

where $\mathcal{D}(\hat{\rho}, \hat{A}_j) = \hat{A}_j \hat{\rho} \hat{A}_j^\dagger - \hat{A}_j^\dagger \hat{A}_j \hat{\rho}/2 - \hat{\rho} \hat{A}_j^\dagger \hat{A}_j/2$ are the dissipators associated with jump operators $\hat{A}_j = \sqrt{\gamma_j'}\hat{a}_j$. Liouvillian EPs (LEPs) are found through the eigenspectra of $\mathcal{L}$ [Fig. 2(b)]. By solving the equation [75] $\mathcal{L}\hat{\rho}_i = \Lambda_i\hat{\rho}_i$, where Λ_i and $\hat{\rho}_i$ are the eigenvalues and the corresponding eigenstates of $\mathcal{L}$. In the one-excitation subspace, LEPs are emerge for $\Lambda_1^+ = \Lambda_1^-$, where $\Lambda_1^\pm$ are the eigenvalues of $\mathcal{L}$. We find that LEP and HEP occur at the same positions, i.e., $\gamma_{\text{tip}}/\gamma_1' = 8.9$, as shown in Figs. 2(a) and 2(b) [75,76].

In addition, we note that, under the semiclassical limit, the eigenvalues of Liouvillian (Λ_i) and the effective non-Hermitian Hamiltonian (λ_i) fulfill $-i(\lambda_l - \lambda_m^*)\hat{\rho}_i = \Lambda_i\hat{\rho}_i$. Thus, the solutions of the Liouvillian and Hamiltonian are different outside of the EPs [Figs. 2(a) and 2(b)].

III. ANALYTICAL AND NUMERICAL RESULTS

In the frame rotating with the driving frequency ω_l, the system's Hamiltonian becomes

$$\hat{H}_r = \sum_{j=1,2} \Delta \hat{a}_j^\dagger \hat{a}_j + \hat{H}_{\text{int}} + \Omega(\hat{a}_1^\dagger + \hat{a}_1), \tag{7}$$

where $\Delta = \omega_c - \omega_l$, and $\Omega = [\gamma_{\text{ex}}P_{\text{in}}/(\hbar\omega_l)]^{1/2}$ is the driving amplitude with power P_{in} on $\mu R1$. Optical losses can be included in the effective non-Hermitian Hamiltonian [77]

$$\hat{H}_{\text{eff}} = \hat{H}_r - i\sum_{j=1,2} (\gamma_j'/2)\hat{a}_j^\dagger \hat{a}_j. \tag{8}$$

Under the weak-driving condition ($\Omega \ll \gamma_1'$), the Hilbert space can be restricted to a subspace with few photons. In the subspace with $N = m + n = 3$ excitations, the general state of the system can be expressed as

$$|\psi(t)\rangle = \sum_{N=0}^{3} \sum_{m=0}^{N} C_{m,N-m}|m, N-m\rangle, \tag{9}$$

with probability amplitudes $C_{m,N-m}$, which can be obtained by solving the Schrödinger equation

$$i|\dot{\psi}(t)\rangle = \hat{H}_{\text{eff}}|\psi(t)\rangle. \tag{10}$$

When a weak-driving field is applied to the cavity, it may excite a few photons in the cavity. Thus, we can approximate the probability amplitudes of the excitations as $C_{m,N-m} \sim (\Omega/\gamma_1')^N$. By using a perturbation method and discarding higher-order terms in each equation for lower-order variables, we obtain the following equations of motion for the probability amplitudes:

$$i\dot{C}_{00}(t) = 0, \quad i\dot{C}_{01}(t) = \Delta_2 C_{01}(t) + J C_{10}(t),$$

$$i\dot{C}_{10}(t) = \Delta_1 C_{10}(t) + J C_{01}(t) + \Omega C_{00}(t),$$

$$i\dot{C}_{02}(t) = 2\Delta_2 C_{02}(t) + \sqrt{2}J C_{11}(t),$$

$$
\begin{aligned}
i\dot{C}_{11}(t) = {} & (\Delta_1 + \Delta_2)C_{11}(t) + \sqrt{2}JC_{20}(t) \\
& + \sqrt{2}JC_{02}(t) + \Omega C_{01}(t), \\
i\dot{C}_{20}(t) = {} & 2\Delta_3 C_{20}(t) + \sqrt{2}JC_{11}(t) + \sqrt{2}\Omega C_{10}(t), \\
i\dot{C}_{03}(t) = {} & 3\Delta_2 C_{03}(t) + \sqrt{3}JC_{12}(t), \\
i\dot{C}_{12}(t) = {} & \Delta_6 C_{12}(t) + 2JC_{21} + \sqrt{3}JC_{03}(t) + \Omega C_{02}(t), \\
i\dot{C}_{21}(t) = {} & \Delta_5 C_{21}(t) + 2JC_{12}(t) + \sqrt{3}JC_{30}(t) \\
& + \sqrt{2}\Omega C_{11}(t), \\
i\dot{C}_{30}(t) = {} & 3\Delta_4 C_{30}(t) + \sqrt{3}JC_{21}(t) + \sqrt{3}\Omega C_{20}(t),
\end{aligned}
\tag{11}
$$

where

$$
\begin{aligned}
\Delta_1 &= \Delta - i\gamma_1'/2, \quad \Delta_2 = \Delta - i\gamma_2'/2, \\
\Delta_3 &= \Delta_1 + \chi, \quad \Delta_4 = \Delta_1 + 2\chi, \\
\Delta_5 &= 2\Delta_3 + \Delta_2, \quad \Delta_6 = \Delta_1 + 2\Delta_2.
\end{aligned}
\tag{12}
$$

For the initially empty resonators, i.e., the initial state of the system is the vacuum state $|00\rangle$, the initial condition reads as $C_{00}(0) = 1$. By setting $\dot{C}_{mn}(t) = 0$, we obtain the following solutions:

$$
\begin{aligned}
C_{01} &= \frac{J\Omega}{\eta_1}, \quad C_{10} = -\frac{\Omega\Delta_2}{\eta_1}, \quad C_{02} = \frac{\sqrt{2}\Omega^2 J^2 \zeta_2}{\eta_1 \eta_2}, \\
C_{11} &= \frac{-2\Omega^2 \Delta_2 J \zeta_2}{\eta_1 \eta_2}, \quad C_{20} = \frac{\sqrt{2}\Omega^2 \Delta_2^2 \zeta_1}{\eta_1 \eta_2}, \\
C_{03} &= \frac{\sqrt{6}J^3 \Omega^3 [2\Delta_2^2 \zeta_1 - \xi_2 \zeta_2]}{3\eta_1 \eta_2 \mu}, \\
C_{12} &= \frac{\sqrt{2}J^2 \Omega^3 \Delta_2 [\xi_2 \zeta_2 - 2\Delta_2^2 \zeta_1]}{\eta_1 \eta_2 \mu}, \\
C_{21} &= \frac{\sqrt{2}J\Omega^3 \Delta_2^2 [2\Delta_4 \Delta_6 \zeta_2 - \eta_3 \zeta_1]}{\eta_1 \eta_2 \mu}, \\
C_{30} &= \frac{\sqrt{6}\Omega^3 \Delta_2^2 [(4J^2 \Delta_2 + \Delta_5 \eta_3)\zeta_1 - 2J^2 \Delta_6 \zeta_2]}{3\eta_1 \eta_2 \mu},
\end{aligned}
\tag{13}
$$

where

$$
\begin{aligned}
\zeta_1 &= \Delta_1 + \Delta_2, \quad \zeta_2 = \Delta_2 + \Delta_3, \\
\eta_1 &= \Delta_1 \Delta_2 - J^2, \quad \eta_2 = 2\xi_1 \Delta_2 - 2J^2 \Delta_3, \\
\eta_3 &= J^2 - \Delta_2 \Delta_6, \quad \xi_1 = \Delta_1 \Delta_3 + \Delta_2 \Delta_3 - J^2, \\
\xi_2 &= J^2 - 4\Delta_2 \Delta_4 - \Delta_4 \Delta_5, \\
\mu &= J^2 \xi_2 - J^2 \Delta_2 \Delta_6 + \Delta_2 \Delta_4 \Delta_5 \Delta_6.
\end{aligned}
\tag{14}
$$

The probabilities of finding m photons in $\mu R1$ and n photons in $\mu R2$ are given by $P_{mn} = |C_{mn}|^2$. The mean-photon numbers in $\mu R1$ and $\mu R2$ are denoted by N_1 and N_2, respectively, and can be obtained from the above probability distribution as

$$
\begin{aligned}
N_1 &= \langle \hat{a}_1^\dagger \hat{a}_1 \rangle = \sum_{N=0}^{3} \sum_{m=0}^{N} m P_{mn} \simeq \frac{\Omega^2 \Delta_2^2}{\eta_1^2}, \\
N_2 &= \langle \hat{a}_2^\dagger \hat{a}_2 \rangle = \sum_{N=0}^{3} \sum_{n=0}^{N} n P_{mn} \simeq \frac{\Omega^2 J^2}{\eta_1^2}.
\end{aligned}
\tag{15}
$$

The effect of increasing γ_{tip} on N_1 and N_2 is depicted in Fig. 4(a). The equal-time (namely, zero-time-delay) second-order correlation function of $\mu R1$ is written as

$$
g_1^{(2)}(0) = \frac{\langle \hat{a}_1^{\dagger 2} \hat{a}_1^2 \rangle}{\langle \hat{a}_1^\dagger \hat{a}_1 \rangle^2} \simeq \frac{4\eta_1^2 (\Delta_1 + \Delta_2)^2}{\eta_2^2}.
\tag{16}
$$

The approximate equal-time third-order correlation function is written as

$$
\begin{aligned}
g_1^{(3)}(0) &= \frac{\langle \hat{a}_1^{\dagger 3} \hat{a}_1^3 \rangle}{\langle \hat{a}_1^\dagger \hat{a}_1 \rangle^3} \\
&\simeq \frac{4\eta_1^4 [(4J^2 \Delta_2 + \Delta_5 \eta_3)\zeta_1 - 2J^2 \Delta_6 \zeta_2]^2}{\eta_2^2 \mu^2 \Delta_2^2}.
\end{aligned}
\tag{17}
$$

To confirm our analytical results, we numerically study the full quantum dynamics of the system by solving the master equation [78,79]

$$
\dot{\rho} = -i[\hat{H}_r, \hat{\rho}] + \sum_{j=1,2} \frac{\gamma_j'}{2}(2\hat{a}_j \hat{\rho} \hat{a}_j^\dagger - \hat{a}_j^\dagger \hat{a}_j \hat{\rho} - \hat{\rho} \hat{a}_j^\dagger \hat{a}_j).
\tag{18}
$$

Then, $P_{mn} = \langle m, n | \rho_{\text{ss}} | m, n \rangle$ can be obtained from the steady-state solutions ρ_{ss}.

In our work, the experimentally accessible parameters are given by [62–66,80–84]: $V_{\text{eff}} = 100 \ \mu\text{m}^3$, $Q = 2 \times 10^9$, $\chi^{(3)}/\varepsilon_r^2 = 2 \times 10^{-17} \ \text{m}^2/\text{V}^2$ (i.e., $\chi/\gamma_1' = 2.2$), $P_{\text{in}} = 4$ fW, $\lambda = 1550$ nm, and $\gamma_2/\gamma_1' = 0.1$. For the microring resonators, V_{eff} is typically 10^2–$10^4 \ \mu\text{m}^3$ [80,81] and Q was increased up to 10^9–10^{12} [82,83]. The Kerr coefficient can be $\chi^{(3)}/\varepsilon_r^2 = 2 \times 10^{-17} \ \text{m}^2/\text{V}^2$ for the semiconductor materials with GaAs [62,63], and reach $\chi^{(3)}/\varepsilon_r^2 = 2.12 \times 10^{-17} \ \text{m}^2/\text{V}^2$ for the materials with indium tin oxide [64]. Also, $\chi^{(3)}$ can be further enhanced to $2 \times 10^{-11} \ \text{m/V}^2$ by introducing other materials [65,66].

An excellent agreement between the analytical and numerical results is seen in Figs. 1(e) and 1(f). Figure 1(e) shows the classical suppression and revival of N_1. Adding loss below the CP_c ($\gamma_{\text{tip}}/\gamma_1' = 5.3$), N_1 is decreased to 0.003. When the loss exceeds the CP_c, N_1 is revived due to the EP-induced mode coalescence. This loss-induced revival of optical intensity was also experimentally demonstrated in a non-Hermitian double-well device consisting of two coupled waveguides [4].

More importantly, we find the loss-induced suppression and revival of quantum correlation in Fig. 1(f). For $\gamma_{\text{tip}} = 0$, single-PB emerges with $g_1^{(2)}(0) \sim 0.23$. Adding loss annihilates it, where the antibunched single-photon stream is converted into bunched photons. Surprisingly, the antibunched stream recovers by further increasing loss beyond the CP_q ($\gamma_{\text{tip}}/\gamma_1' = 6.5$), and single-PB is fully revived at the EP ($\gamma_{\text{tip}}/\gamma_1' = 8.9$). We also find that the CP_q gradually moves
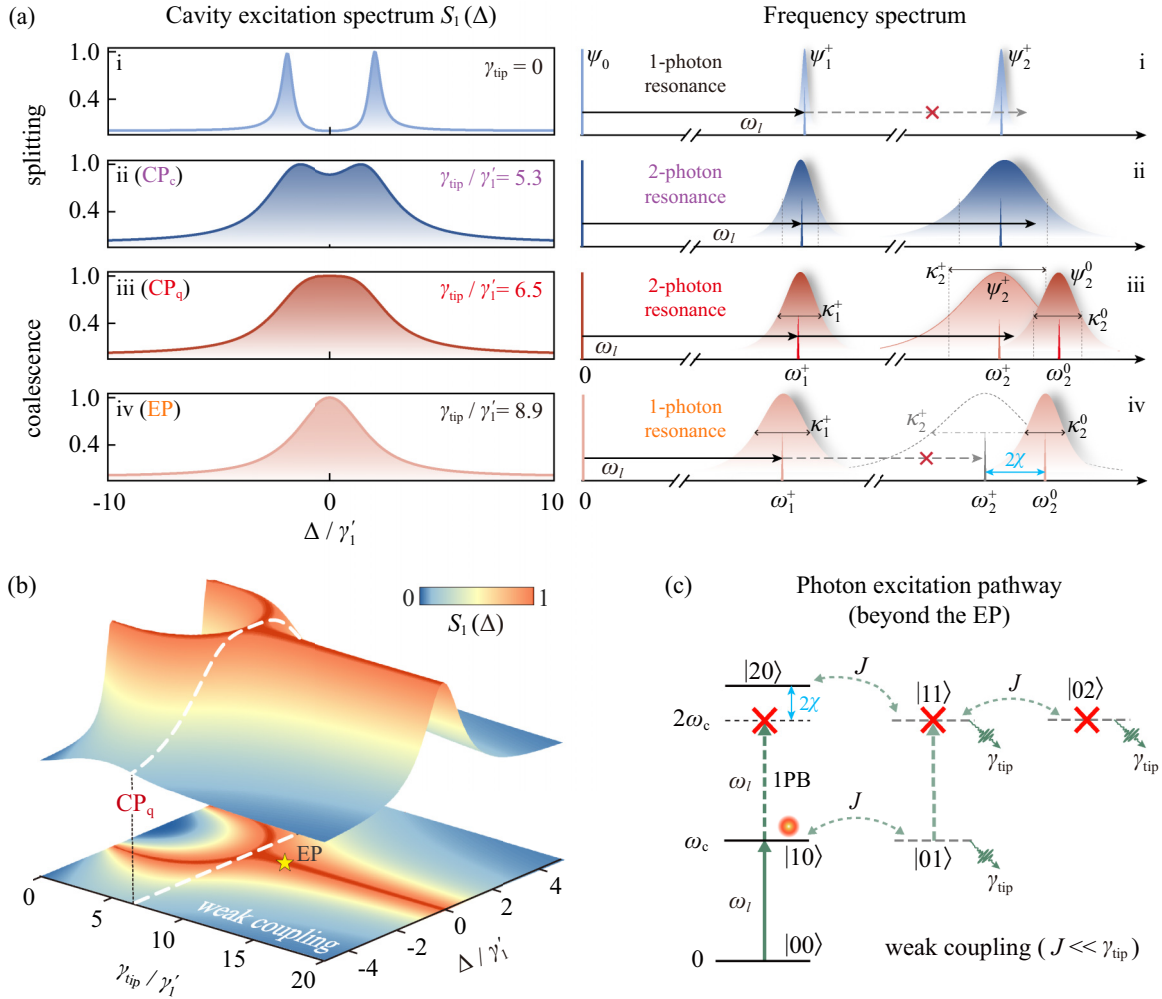
FIG. 3. The origin of loss-induced quantum suppression and revival. (a) The cavity excitation spectra $S_1(\Delta)$ and the eigenfrequency spectra $\omega_{1,2}$ with linewidths $\kappa_{1,2}$ for different critical points. (b) By increasing loss beyond the CP_q the system enters the weak coupling regime featuring unresolved spectra of the two modes. (c) The photon excitation pathway beyond the EP shows the breakdown of two-photon resonance, leading to the full revival of single-PB. The dashed arrows are the forbidden excitations.

away from EP as the system moves closer to the thermodynamic limit [85] (see details in Appendix C).

This loss-induced revival of single-PB requires the interplay of both EP-induced mode coalescence and the breakdown of two-photon resonance. We study the mode splitting and coalescence in the cavity excitation spectrum of $\mu R1$:

$$S_1(\Delta) = \frac{N_1}{n_0} \simeq \frac{(\gamma_1' + \gamma_2')^2 \Delta_2^2}{\eta_1^2}, \qquad (19)$$

where $n_0 = \Omega^2/(\gamma_1' + \gamma_2')^2$ is the normalization factor. We find that the cavity excitation spectrum becomes coalescent at the quantum critical point CP_q [Figs. 2(c) and 3(a) and 3(b)]. In the mode-splitting region, the light with frequency ω_1^+ is resonantly coupled to the transition $|\psi_0\rangle \rightarrow |\psi_1^+\rangle$, while $|\psi_1^+\rangle \rightarrow |\psi_2^+\rangle$ is detuned, resulting in single-PB at $\gamma_{\text{tip}} = 0$ [Fig. 3(a-i)]. By further adding γ_{tip}, the light coincides with the two-photon resonance, leading to a suppression of single-PB. The CP_c is in the quantum suppression process with two separated modes, and fulfills the condition of two-photon resonance [Fig. 3(a-ii)].

Increasing γ_{tip} to CP_q leads to an overlap of the two modes [Fig. 3(a-iii)], indicating the two cavities enter the effective weak-coupling regime ($J \ll \gamma_{\text{tip}}$) [Fig. 3(b)]. This process breaks two-photon resonance resulting in the revival of single-photon resonance. Eventually, two modes coalesce at EP, and the single-photon resonance fully recovers leading to single-PB [Fig. 3(a-iv)]. We note that the CP_q features the transition from two separated modes to an overlap of the two modes, as well as the transition from two-photon resonance to single-photon resonance.

Specifically, by increasing loss beyond the EP, $|\psi_2^+\rangle$ and $|\psi_2^-\rangle$ are localized on $|0, 2\rangle$ and $|1, 1\rangle$, respectively [Fig. 4(c)]. Although $|0, 2\rangle$ or $|1, 1\rangle$ coincides with the two-photon resonance energy $2\omega_c$, the transitions from $|0, 0\rangle$ to $|0, 2\rangle$ and $|1, 1\rangle$, i.e., $|\psi_0\rangle \rightarrow |\psi_2^\pm\rangle$, are forbidden due to the effective weak coupling between the two cavities [Fig. 3(c)]. Here, $|\psi_2^0\rangle$ and $|\psi_1^+\rangle$ are governed by the states $|2, 0\rangle$ and $|1, 0\rangle$, respectively [Figs. 4(b) and 4(c)]. When the light resonantly coupled to $|0, 0\rangle \rightarrow |1, 0\rangle$, the transition $|1, 0\rangle \rightarrow |2, 0\rangle$ is detuned by 2χ, i.e., single-PB is revived.
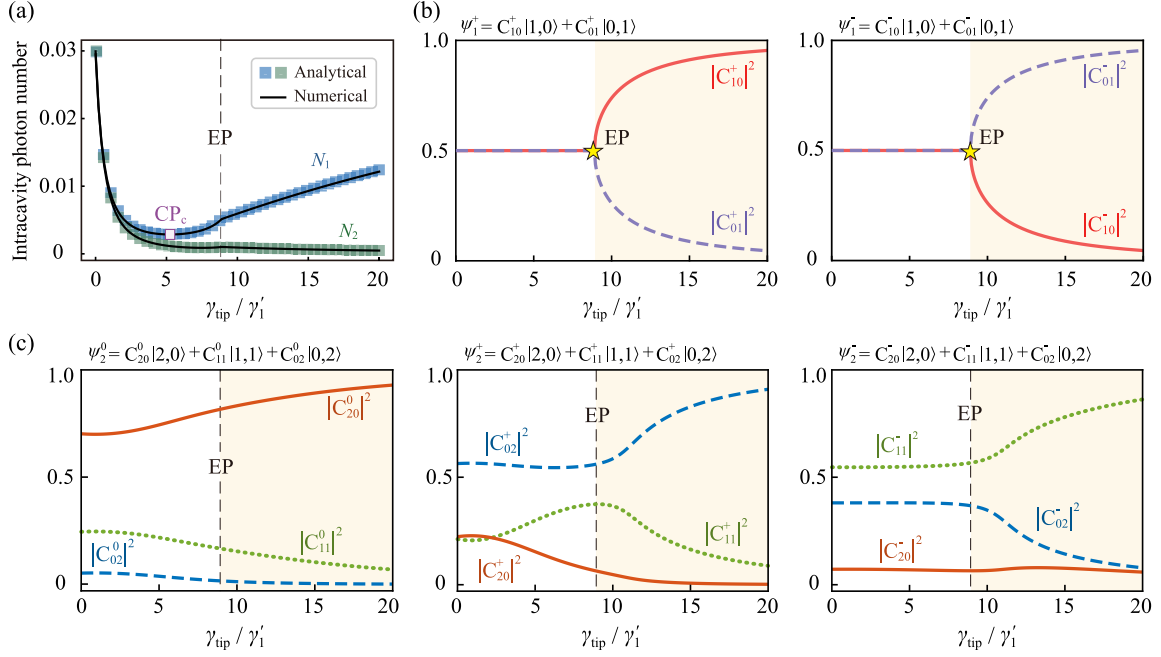
FIG. 4. (a) Intracavity photon numbers N_1 (blue) and N_2 (green) versus γ_{tip}. Below CP_c, N_1 and N_2 decrease by increasing γ_{tip}. When γ_{tip} exceeds CP_c, N_1 is revived, while N_2 keep decreasing, resulting in a predominant mode localized in $\mu R1$. The analytical results (colored squares) agree well with the numerical results (black solid curves). After the EP, (b) the single-photon eigenstates $|\psi_1^{\pm}\rangle$ are intensively localized on $|1,0\rangle$ and $|0,1\rangle$, respectively. (c) The $|\psi_2^{0,\pm}\rangle$ are, respectively, governed by the states $|2,0\rangle$, $|0,2\rangle$, and $|1,1\rangle$.

We conclude that the interplay of EP-induced mode coalescence and the breakdown of two-photon resonance leads to this loss-induced quantum revival of single PB. This underlying principle is different from that of loss-induced entanglement [86] in which a quantum effect is realized through conditional dynamics.

Figure 5 shows different quantum correlations can be tuned by adding loss for the revived light after CP_c. Single-PB features two-photon antibunching, while two-PB features three-photon antibunching, but with two-photon bunching, i.e., the absorption of two photons can suppress the absorption of additional photons [26]. Two-PB fulfills the conditions [11]: $g_1^{(3)}(0) < 1$ and $g_1^{(2)}(0) > 1$, with $g_1^{(3)}(0) = \langle \hat{a}_1^{\dagger 3} \hat{a}_1^3 \rangle / \langle \hat{a}_1^{\dagger} \hat{a}_1 \rangle^3$.

We find two-PB emerges with $g_1^{(3)}(0) \sim 0.27$ and $g_1^{(2)}(0) \sim 1.12$ at $\gamma_{\text{tip}}/\gamma_1' = 6$ [Fig. 5(a)]. Adding γ_{tip} beyond CP_q leads to a single-PB occurring at the EP. These results can also be confirmed by comparing the photon-number distribution P_m with the Poisson distribution $\mathcal{P}_m$ [Fig. 5(b)]. We find that two-photon probability P_2 is enhanced while $P_{m>2}$ are suppressed at $\gamma_{\text{tip}}/\gamma_1' = 6$, which is in sharp contrast to the case at the EP. With such a device, a switch between two-PB and single-PB can be achieved by tuning loss below or beyond CP_q.

IV. MORE COMPARISONS AND DISCUSSIONS

We now present some discussions on the comparison with single-mode systems. If one only considers a single-mode system, i.e., by placing a nanotip near a single resonator, it is impossible to observe the classical HEP or the classical effect of LIT. Moreover, although single-PB can be realized in

single-mode systems [28,87], the loss-induced revival effects cannot be revealed in the single-mode systems due to the absence of the EP, in which both the mean photon number and quantum correlations are suppressed by increasing loss [Figs. 6(a) and 6(b)].
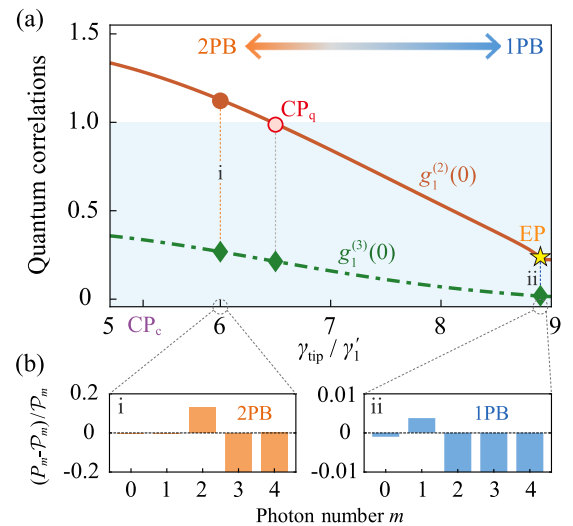

FIG. 5. Loss-induced quantum switching between two-photon blockade (2PB) and single-photon blockade (1PB). (a) $g_1^{(2)}(0)$ (red solid curve) and $g_1^{(3)}(0)$ (green dashed curve) versus γ_{tip}. (b) This quantum switch can also be recognized from the deviations of the photon distribution P_m to the standard Poisson distribution $\mathcal{P}_m$ with the same mean photon number m.
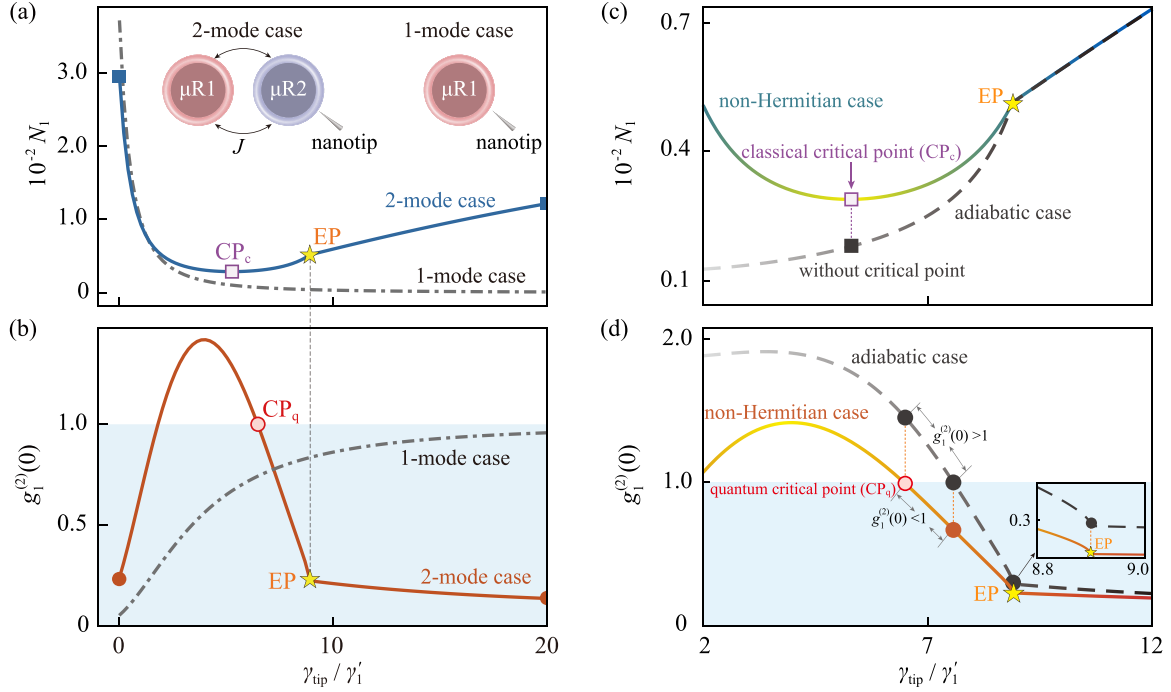
FIG. 6. (a) The intracavity photon number N_1 and (b) the second-order correlation function $g_1^{(2)}(0)$ versus $\gamma_{\rm tip}$ for single-mode (dot-dashed curves) and two-mode (solid curves) cases. (c) N_1 and (d) $g_1^{(2)}(0)$ versus $\gamma_{\rm tip}$ in different methods. The black dashed (color solid) is obtained for the adiabatic case (non-Hermitian case).

In addition, we give a comparison between the adiabatic elimination and the EP case. The Heisenberg equations of motion of this compound system are

$$\dot{a}_1 = -i\Delta_0 \hat{a}_1 - \frac{\gamma_1'}{2}\hat{a}_1 - 2i\chi \hat{a}_1^\dagger \hat{a}_1 \hat{a}_1 - iJ\hat{a}_2 - i\Omega,$$

$$\dot{a}_2 = -i\Delta_0 \hat{a}_2 - \frac{\gamma_2'}{2}\hat{a}_2 - iJ\hat{a}_1. \qquad (20)$$

We now suppose that $\gamma_{\rm tip}$ is large and adiabatically eliminate mode a_2. A widely used prescription for this is to set $\dot{a}_2$ to zero and solve the resulting equations for $\hat{a}_2$ [88], so eliminating $\hat{a}_2$ from the remaining equation of Eq. (20). The result is

$$\dot{a}_1 = -i\Delta_0 \hat{a}_1 - \frac{\gamma_1'}{2}\hat{a}_1 - 2i\chi \hat{a}_1^\dagger \hat{a}_1 \hat{a}_1$$

$$- \frac{J^2}{i\Delta_0 + \gamma_2'/2}\hat{a}_1 - i\Omega. \qquad (21)$$

By comparing the Eqs. (20) and (21), we see that the coupling of cavity mode a_1 to cavity mode a_2 can essentially be regarded as adding an additional loss channel for cavity $\mu R1$ for large $\gamma_{\rm tip}$. This is not a large increase in the loss of mode a_1, and of course the increase becomes less and less with increasing $\gamma_{\rm tip}$.

We find that the adiabatic elimination method can not provide a good description before EP for neither the mean-photon number N_1 nor the quantum correlation function $g_1^{(2)}(0)$, as shown in Figs. 6(c) and 6(d). Specifically, (i) the EP can lead to classical suppression and revival of N_1, and classical critical point (CP_c), i,e., the minimum of the classical N_1. However, in the adiabatic case, there is no turning point for

N_1 by continuously increasing $\gamma_{\rm tip}$ [Fig. 6(c)]. For quantum correlations, the adiabatic elimination method fails to reveal the suppression process by increasing loss [Fig. 6(d)]. (ii) The adiabatic elimination method also fails to show the revival process by increasing loss to the vicinity of the quantum critical point (CP_q), where $g_1^{(2)}(0) > 1$ for the adiabatic case [Fig. 6(d)]. (iii) At the EP, the value of $g_1^{(2)}(0)$ for the adiabatic case is 27% higher than that for our EP theory.

V. CONCLUSION

In summary, we show how to engineer quantum correlations with the help of loss, which is in contrast to the general belief that nonclassical correlations are fragile and can be destroyed by loss. Our findings contain three main features. First, previous works on LIT [4–6] mainly focused on the classical regime, i.e., studying the optical intensities instead of quantum correlations. Our work here fills this gap and reveals unexpected purely quantum features of the LIT. Furthermore, in contrast to the classical LIT resulting from EPs, the underlying physical mechanism of such a purely quantum revival effect is not only the EP-induced mode coalescence, but also the breakdown of two-photon resonance. More interestingly, different types of quantum correlations are exhibited in the revived light, which can be well tuned by loss. This ability provides a counterintuitive possibility for achieving quantum switches of photons by harnessing the power of loss.

Our work sheds light on reversing the effect of loss in the fully quantum regime, which not only facilitates the fundamental studies of quantum physics with lossy materials or topological structures [89–93], but also provides possibilities

to achieve loss-tuned quantum devices for applications in quantum engineering.

APPENDIX A: ANALYTICAL SOLUTION FOR HAMILTONIAN EXCEPTIONAL POINT

The nonlinear eigenenergy spectrum can be obtained through the following Hamiltonian:

$$\hat{H} = \hat{H}_i - i\frac{\gamma_1'}{2}\hat{a}_1^\dagger \hat{a}_1 - i\frac{\gamma_2'}{2}\hat{a}_2^\dagger \hat{a}_2. \tag{A1}$$

Since the commutative relation $[\hat{a}_1^\dagger \hat{a}_1 + \hat{a}_2^\dagger \hat{a}_2, \hat{H}] = 0$, the total excitation number is conserved, we can obtain the eigensystem with the Hilbert space spanned by the basis state $|m, n\rangle$, i.e., the Fock state with m photons in $\mu R1$ and n photons in $\mu R2$.

In the zero-excitation subspace, we have $\hat{H}\psi_0 = \lambda_0\psi_0$, and the eigenstate is given by $\psi_0 = |0, 0\rangle$ with the eigenvalue $\lambda_0 = 0$. In this subspace with one photon, the Hamiltonian can be expressed as

$$\hat{H} = \begin{pmatrix} \omega_c - i\frac{\gamma_1'}{2} & J \\ J & \omega_c - i\frac{\gamma_2'}{2} \end{pmatrix}. \tag{A2}$$

The complex eigenvalues are

$$\lambda_1^\pm = -i\Gamma + \omega_c \pm \sqrt{J^2 - \beta^2}, \tag{A3}$$

whose real and imaginary parts indicate the eigenfrequencies $\omega_1^\pm$ and the linewidths $\kappa_1^\pm$, respectively. Here, $\Gamma = (\gamma_1' + \gamma_2')/4$ and $\beta = (\gamma_2' - \gamma_1')/4$ quantify the total loss and the loss contrast of the system, respectively. The Hamiltonian EPs (HEPs) are defined as the spectral degeneracies of the non-Hermitian Hamiltonian [51], which emerge for $\lambda_1^+ = \lambda_1^-$, i.e.,

$$\gamma_{\text{tip}}^{\text{EP}} = 4J + \gamma_1' - \gamma_2. \tag{A4}$$

The corresponding eigenstates are

$$\psi_1^\pm = C_{10}^\pm|1, 0\rangle + C_{01}^\pm|0, 1\rangle, \tag{A5}$$

where

$$C_{10}^\pm = J\mathcal{N}_1^\pm,$$
$$C_{01}^\pm = -(i\beta \mp \sqrt{J^2 - \beta^2})\mathcal{N}_1^\pm,$$
$$\mathcal{N}_1^\pm = (|J|^2 + |i\beta \mp \sqrt{J^2 - \beta^2}|^2)^{-1/2}. \tag{A6}$$

In this subspace with two photons, we express the Hamiltonian in the matrix form as

$$\hat{H} = \begin{pmatrix} 2\omega_c + 2\chi - i\gamma_1' & \sqrt{2}J & 0 \\ \sqrt{2}J & 2\omega_c - i\frac{\gamma_1' + \gamma_2'}{2} & \sqrt{2}J \\ 0 & \sqrt{2}J & 2\omega_c - i\gamma_2' \end{pmatrix}. \tag{A7}$$

By solving the characteristic equation, we find the eigenvalues as

$$\lambda_2^0 = G - \frac{(1 - i\sqrt{3})E}{3 \times 2^{2/3}F} + \frac{(1 + i\sqrt{3})F}{6 \times 2^{1/3}},$$

$$\lambda_2^+ = G - \frac{(1 + i\sqrt{3})E}{3 \times 2^{2/3}F} + \frac{(1 - i\sqrt{3})F}{6 \times 2^{1/3}}, \tag{A8}$$

$$\lambda_2^- = G + \frac{2^{1/3}E}{3F} - \frac{F}{3 \times 2^{1/3}},$$

where

$$A = 2\omega_c + 2\chi - i\gamma_1',$$

$$B = 2\omega_c - i\frac{\gamma_1' + \gamma_2'}{2}, \quad C = 2\omega_c - i\gamma_2',$$

$$D = 36J^2\chi + \frac{9}{2}\chi(\gamma_1' - \gamma_2')^2 + 18i\chi^2(\gamma_1' - \gamma_2') - 16\chi^3,$$

$$E = -12J^2 + \frac{3}{4}(\gamma_1' - \gamma_2')^2 + 3i\chi(\gamma_1' - \gamma_2') - 4\chi^2,$$

$$F = [D + \sqrt{4E^3 + D^2}]^{1/3}, \quad G = \frac{1}{3}(A + B + C), \tag{A9}$$

whose real and imaginary parts are the eigenfrequencies $\omega_2^{\pm,0}$ and the linewidths $\kappa_2^{\pm,0}$, respectively. The corresponding eigenstates are

$$\psi_2^{\pm,0} = C_{20}^{\pm,0}|2, 0\rangle + C_{11}^{\pm,0}|1, 1\rangle + C_{02}^{\pm,0}|0, 2\rangle, \tag{A10}$$

where

$$C_{20}^{\pm,0} = \sqrt{2}J(C - \lambda_2^{\pm,0})\mathcal{N}_2^{\pm,0},$$
$$C_{11}^{\pm,0} = -(C - \lambda_2^{\pm,0})|A - \lambda_2^{\pm,0}|\mathcal{N}_2^{\pm,0},$$
$$C_{02}^{\pm,0} = \sqrt{2}J|A - \lambda_2^{\pm,0}|\mathcal{N}_2^{\pm,0},$$
$$\mathcal{N}_2^{\pm,0} = [2J^2(|C - \lambda_2^{\pm,0}|^2 + |A - \lambda_2^{\pm,0}|^2)$$
$$+ |A - \lambda_2^{\pm,0}|^2|C - \lambda_2^{\pm,0}|^2]^{-1/2}. \tag{A11}$$

APPENDIX B: PASSIVE PARITY-TIME SYMMETRY

In our scheme, we consider two passive coupled resonators. This system is identified as passive parity-time (PT) symmetric systems [3]. The system consisting of two lossy components is represented by a 2×2 matrix [as done in Eq. (A2)]. The corresponding Schrödinger equation is given as follows ($\hbar = 1$):

$$i\frac{d}{dt}\begin{pmatrix} \hat{a}_1 \\ \hat{a}_2 \end{pmatrix} = \begin{pmatrix} \omega_c - i\frac{\gamma_1'}{2} & J \\ J & \omega_c - i\frac{\gamma_2'}{2} \end{pmatrix}\begin{pmatrix} \hat{a}_1 \\ \hat{a}_2 \end{pmatrix}. \tag{B1}$$

Defining $\Gamma = (\gamma_1' + \gamma_2')/4$ and $\beta = (\gamma_2' - \gamma_1')/4$, and applying the gauge transformation

$$(\hat{a}_1 \quad \hat{a}_2)^T = e^{-\Gamma t}(\hat{a}_1' \quad \hat{a}_2')^T, \tag{B2}$$

we end up with

$$i\frac{d}{dt}\begin{pmatrix}\hat{a}_1' \\ \hat{a}_2'\end{pmatrix} = \begin{pmatrix} \omega_c - i\frac{\gamma_1'}{2} & J \\ J & \omega_c - i\frac{\gamma_2'}{2} \end{pmatrix}\begin{pmatrix}\hat{a}_1' \\ \hat{a}_2'\end{pmatrix} + i\Gamma\begin{pmatrix}\hat{a}_1' \\ \hat{a}_2'\end{pmatrix}$$

$$= \begin{pmatrix} \omega_c + i\beta & J \\ J & \omega_c - i\beta \end{pmatrix}\begin{pmatrix}\hat{a}_1' \\ \hat{a}_2'\end{pmatrix}$$

$$= \hat{H}'\begin{pmatrix}\hat{a}_1' \\ \hat{a}_2'\end{pmatrix}. \qquad (B3)$$

The off-diagonal elements J in the effective Hamiltonian $\hat{H}'$ are the same as those in the original Hamiltonian $\hat{H}$; however, the imaginary parts of the diagonal elements are now balanced, which means that the magnitude of the gain in the one of the diagonal elements is equal to that in the other diagonal element. This matrix fulfills $[\hat{H}', PT] = 0$ and thus it is PT symmetric.

Thus, the gauge transformation reveals the hidden PT symmetry present in the non-Hermitian matrix $\hat{H}$ by changing the reference point (see details in Ref. [3]).

APPENDIX C: QUANTUM CRITICAL POINT IN THE THERMODYNAMIC LIMIT

The thermodynamic limit is obtained by letting the nonlinearity go to 0 and the driving intensity go to $+\infty$ while
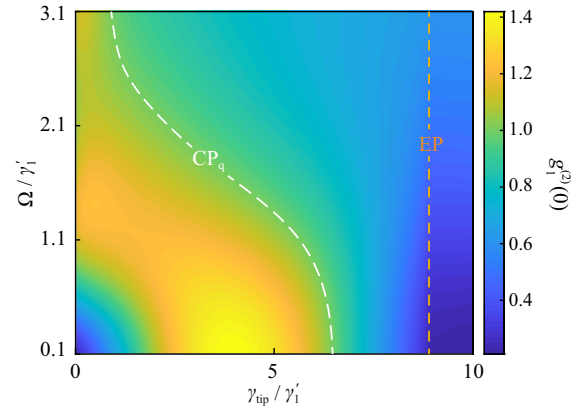

FIG. 7. The second-order correlation function $g_1^{(2)}(0)$ obtained as function of γ_{tip} and Ω. The white dashed indicates CP_q.

keeping their product constant [85]. However, in our system, the generation of the conventional photon blockade requires large nonlinearity and weak drive strength. Thus, in the thermodynamic limit, it is almost impossible to generate the conventional photon blockade. As shown in Fig. 7, the second-order correlation function $g_1^{(2)}(0)$ is increased with increasing driving strength Ω, which is not conducive to the generation of PB. Even when the Ω is large enough, the photon blockade will disappear. Moreover, we found that CP_q gradually moved away from EP with increasing Ω [Fig. 7].

[1] C. M. Bender, Rep. Prog. Phys. **70**, 947 (2007).

[2] R. El-Ganainy, M. Khajavikhan, D. N. Christodoulides, and Ş. K. Özdemir, Commun. Phys. **2**, 37 (2019).

[3] Ş. K. Özdemir, S. Rotter, F. Nori, and L. Yang, Nat. Mater. **18**, 783 (2019).

[4] A. Guo, G. J. Salamo, D. Duchesne, R. Morandotti, M. Volatier-Ravat, V. Aimez, G. A. Siviloglou, and D. N. Christodoulides, Phys. Rev. Lett. **103**, 093902 (2009).

[5] H. Zhang, F. Saif, Y. Jiao, and H. Jing, Opt. Express **26**, 25199 (2018).

[6] B. Peng, Ş. K. Özdemir, S. Rotter, H. Yilmaz, M. Liertzer, F. Monifi, C. M. Bender, F. Nori, and L. Yang, Science **346**, 328 (2014).

[7] X. Huang, C. Lu, C. Liang, H. Tao, and Y.-C. Liu, Light Sci. Appl. **10**, 30 (2021).

[8] S. Dong, G. Hu, Q. Wang, Y. Jia, Q. Zhang, G. Cao, J. Wang, S. Chen, D. Fan, W. Jiang, Y. Li, A. Alù, and C.-W. Qiu, ACS Photonics **7**, 3321 (2020).

[9] K. M. Birnbaum, A. Boca, R. Miller, A. D. Boozer, T. E. Northup, and H. J. Kimble, Nature (London) **436**, 87 (2005).

[10] A. Faraon, I. Fushman, D. Englund, N. Stoltz, P. Petroff, and J. Vučković, Nat. Phys. **4**, 859 (2008).

[11] C. Hamsen, K. N. Tolazzi, T. Wilk, and G. Rempe, Phys. Rev. Lett. **118**, 133604 (2017).

[12] H. J. Snijders, J. A. Frey, J. Norman, H. Flayac, V. Savona, A. C. Gossard, J. E. Bowers, M. P. van Exter, D. Bouwmeester, and W. Löffler, Phys. Rev. Lett. **121**, 043601 (2018).

[13] C. Vaneph, A. Morvan, G. Aiello, M. Féchant, M. Aprili, J. Gabelli, and J. Estève, Phys. Rev. Lett. **121**, 043602 (2018).

[14] C. Lang, D. Bozyigit, C. Eichler, L. Steffen, J. M. Fink, A. A. Abdumalikov, M. Baur, S. Filipp, M. P. da Silva, A. Blais, and A. Wallraff, Phys. Rev. Lett. **106**, 243601 (2011).

[15] A. J. Hoffman, S. J. Srinivasan, S. Schmidt, L. Spietz, J. Aumentado, H. E. Türeci, and A. A. Houck, Phys. Rev. Lett. **107**, 053602 (2011).

[16] T. Peyronel, O. Firstenberg, Q.-Y. Liang, S. Hofferberth, A. V. Gorshkov, T. Pohl, M. D. Lukin, and V. Vuletić, Nature (London) **488**, 57 (2012).

[17] A. Imamoglu, H. Schmidt, G. Woods, and M. Deutsch, Phys. Rev. Lett. **79**, 1467 (1997).

[18] P. Rabl, Phys. Rev. Lett. **107**, 063601 (2011).

[19] J.-Q. Liao and F. Nori, Phys. Rev. A **88**, 023853 (2013).

[20] X.-Y. Lü, Y. Wu, J. R. Johansson, H. Jing, J. Zhang, and F. Nori, Phys. Rev. Lett. **114**, 093602 (2015).

[21] H. Wang, X. Gu, Y.-x. Liu, A. Miranowicz, and F. Nori, Phys. Rev. A **92**, 033806 (2015).

[22] G.-L. Zhu, X.-Y. Lü, L.-L. Wan, T.-S. Yin, Q. Bin, and Y. Wu, Phys. Rev. A **97**, 033830 (2018).

[23] F. Zou, L.-B. Fan, J.-F. Huang, and J.-Q. Liao, Phys. Rev. A **99**, 043837 (2019).

[24] C. Zhai, R. Huang, H. Jing, and L.-M. Kuang, Opt. Express **27**, 27649 (2019).

[25] S. S. Shamailov, A. S. Parkins, M. J. Collett, and H. J. Carmichael, Opt. Commun. **283**, 766 (2010).

[26] A. Miranowicz, M. Paprzycka, Y.-X. Liu, J. Bajer, and F. Nori, Phys. Rev. A **87**, 023809 (2013).

[27] Q. Bin, X.-Y. Lü, S.-W. Bin, and Y. Wu, Phys. Rev. A **98**, 043858 (2018).

[28] S. Ghosh and T. C. H. Liew, Phys. Rev. Lett. **123**, 013602 (2019).

[29] D. Roberts and A. A. Clerk, Phys. Rev. X **10**, 021022 (2020).

[30] J.-B. You, X. Xiong, P. Bai, Z.-K. Zhou, R.-M. Ma, W.-L. Yang, Y.-K. Lu, Y.-F. Xiao, C. E. Png, F. J. Garcia-Vidal, C.-W. Qiu, and L. Wu, Nano Lett. **20**, 4645 (2020).

[31] B. Dayan, A. S. Parkins, T. Aoki, E. P. Ostby, K. J. Vahala, and H. J. Kimble, Science **319**, 1062 (2008).

[32] I. Shomroni, S. Rosenblum, Y. Lovsky, O. Bechler, G. Guendelman, and B. Dayan, Science **345**, 903 (2014).

[33] M. Scheucher, A. Hilico, E. Will, J. Volz, and A. Rauschenbeutel, Science **354**, 1577 (2016).

[34] J. Jin, D. Rossini, R. Fazio, M. Leib, and M. J. Hartmann, Phys. Rev. Lett. **110**, 163605 (2013).

[35] A. D. Greentree, C. Tahan, J. H. Cole, and L. C. L. Hollenberg, Nat. Phys. **2**, 856 (2006).

[36] D. G. Angelakis, M. F. Santos, and S. Bose, Phys. Rev. A **76**, 031805(R) (2007).

[37] C. Noh and D. G. Angelakis, Rep. Prog. Phys. **80**, 016401 (2017).

[38] S. Zeytinoğlu and A. İmamoğlu, Phys. Rev. A **98**, 051801(R) (2018).

[39] I. Pietikäinen, J. Tuorila, D. S. Golubev, and G. S. Paraoanu, Phys. Rev. A **99**, 063828 (2019).

[40] O. Kyriienko, D. N. Krizhanovskii, and I. A. Shelykh, Phys. Rev. Lett. **125**, 197402 (2020).

[41] O. A. Iversen and T. Pohl, Phys. Rev. Lett. **126**, 083605 (2021).

[42] A. Ridolfo, M. Leib, S. Savasta, and M. J. Hartmann, Phys. Rev. Lett. **109**, 193602 (2012).

[43] Y.-X. Liu, X.-W. Xu, A. Miranowicz, and F. Nori, Phys. Rev. A **89**, 043818 (2014).

[44] R. Huang, A. Miranowicz, J.-Q. Liao, F. Nori, and H. Jing, Phys. Rev. Lett. **121**, 153601 (2018).

[45] T. C. H. Liew and V. Savona, Phys. Rev. Lett. **104**, 183601 (2010).

[46] M. Bamba, A. Imamoğlu, I. Carusotto, and C. Ciuti, Phys. Rev. A **83**, 021802(R) (2011).

[47] A. Majumdar, M. Bajcsy, A. Rundquist, and J. Vučković, Phys. Rev. Lett. **108**, 183601 (2012).

[48] H. Flayac and V. Savona, Phys. Rev. A **96**, 053810 (2017).

[49] F. Zou, D.-G. Lai, and J.-Q. Liao, Opt. Express **28**, 16175 (2020).

[50] B. Li, R. Huang, X. Xu, A. Miranowicz, and H. Jing, Photon. Res. **7**, 630 (2019).

[51] M.-A. Miri and A. Alù, Science **363**, eaar7709 (2019).

[52] S. Feng, Phys. Rev. Lett. **108**, 193904 (2012).

[53] V. I. Fesenko and V. R. Tuz, Phys. Rev. B **99**, 094404 (2019).

[54] X. Qiao, B. Midya, Z. Gao, Z. Zhang, H. Zhao, T. Wu, J. Yim, R. Agarwal, N. M. Litchinitser, and L. Feng, Science **372**, 403 (2021).

[55] S. E. Harris and Y. Yamamoto, Phys. Rev. Lett. **81**, 3611 (1998).

[56] D. E. Chang, A. S. Sørensen, E. A. Demler, and M. D. Lukin, Nat. Phys. **3**, 807 (2007).

[57] A. Kubanek, A. Ourjoumtsev, I. Schuster, M. Koch, P. W. H. Pinkse, K. Murr, and G. Rempe, Phys. Rev. Lett. **101**, 203602 (2008).

[58] D. Fattal, K. Inoue, J. Vučković, C. Santori, G. S. Solomon, and Y. Yamamoto, Phys. Rev. Lett. **92**, 037903 (2004).

[59] I. Buluta and F. Nori, Science **326**, 108 (2009).

[60] I. M. Georgescu, S. Ashhab, and F. Nori, Rev. Mod. Phys. **86**, 153 (2014).

[61] W. Zhao, S.-D. Zhang, A. Miranowicz, and H. Jing, Sci. China Phys. Mech. Astron. **63**, 224211 (2020).

[62] J. M. Hales, S.-H. Chi, T. Allen, S. Benis, N. Munera, J. W. Perry, D. McMorrow, D. J. Hagan, and E. W. Van Stryland, in *CLEO: Science and Innovations* (Optical Society of America, Washington, D.C., 2018), pp. JTu2A–59.

[63] M. Heuck, K. Jacobs, and D. R. Englund, Phys. Rev. Lett. **124**, 160501 (2020).

[64] M. Z. Alam, I. De Leon, and R. W. Boyd, Science **352**, 795 (2016).

[65] J. A. Zielińska and M. W. Mitchell, Opt. Lett. **42**, 5298 (2017).

[66] H. Choi, M. Heuck, and D. Englund, Phys. Rev. Lett. **118**, 223605 (2017).

[67] G. Kirchmair, B. Vlastakis, Z. Leghtas, S. E. Nigg, H. Paik, E. Ginossar, M. Mirrahimi, L. Frunzio, S. M. Girvin, and R. J. Schoelkopf, Nature (London) **495**, 205 (2013).

[68] X. Gu, A. F. Kockum, A. Miranowicz, Y.-X. Liu, and F. Nori, Phys. Rep. **718-719**, 1 (2017).

[69] K. Xia, F. Nori, and M. Xiao, Phys. Rev. Lett. **121**, 203602 (2018).

[70] Z. R. Gong, H. Ian, Y.-x. Liu, C. P. Sun, and F. Nori, Phys. Rev. A **80**, 065801 (2009).

[71] X.-Y. Lü, W.-M. Zhang, S. Ashhab, Y. Wu, and F. Nori, Sci. Rep. **3**, 2943 (2013).

[72] Y.-P. Wang, G.-Q. Zhang, D. Zhang, T.-F. Li, C.-M. Hu, and J. Q. You, Phys. Rev. Lett. **120**, 057202 (2018).

[73] G.-Q. Zhang, Z. Chen, D. Xu, N. Shammah, M. Liao, T.-F. Li, L. Tong, S.-Y. Zhu, F. Nori, and J. Q. You, PRX Quantum **2**, 020307 (2021).

[74] M. A. Quiroz-Juárez, A. Perez-Leija, K. Tschernig, B. M. Rodríguez-Lara, O. S. Magaña Loaiza, K. Busch, Y. N. Joglekar, and R. J. León-Montiel, Photon. Res. **7**, 862 (2019).

[75] F. Minganti, A. Miranowicz, R. W. Chhajlany, and F. Nori, Phys. Rev. A **100**, 062131 (2019).

[76] R. Huang, Ş. K. Özdemir, J.-Q. Liao, F. Minganti, L.-M. Kuang, F. Nori, and H. Jing, Laser Photonics Rev. **16**, 2100430 (2022).

[77] M. B. Plenio and P. L. Knight, Rev. Mod. Phys. **70**, 101 (1998).

[78] J. R. Johansson, P. D. Nation, and F. Nori, Comput. Phys. Commun. **183**, 1760 (2012).

[79] J. R. Johansson, P. D. Nation, and F. Nori, Comput. Phys. Commun. **184**, 1234 (2013).

[80] K. J. Vahala, Nature (London) **424**, 839 (2003).

[81] S. M. Spillane, T. J. Kippenberg, K. J. Vahala, K. W. Goh, E. Wilcut, and H. J. Kimble, Phys. Rev. A **71**, 013817 (2005).

[82] N. G. Pavlov, G. Lihachev, S. Koptyaev, E. Lucas, M. Karpov, N. M. Kondratiev, I. A. Bilenko, T. J. Kippenberg, and M. L. Gorodetsky, Opt. Lett. **42**, 514 (2017).

[83] V. Huet, A. Rasoloniaina, P. Guillemé, P. Rochard, P. Féron, M. Mortier, A. Levenson, K. Bencheikh, A. Yacomotti, and Y. Dumeige, Phys. Rev. Lett. **116**, 133902 (2016).

[84] I. Schuster, A. Kubanek, A. Fuhrmanek, T. Puppe, P. W. H. Pinkse, K. Murr, and G. Rempe, Nat. Phys. **4**, 382 (2008).

[85] W. Casteels, R. Fazio, and C. Ciuti, Phys. Rev. A **95**, 012128 (2017).

[86] M. B. Plenio, S. F. Huelga, A. Beige, and P. L. Knight, Phys. Rev. A **59**, 2468 (1999).

[87] S. Ferretti and D. Gerace, Phys. Rev. B **85**, 033303 (2012).

[88] M. Fewell, Opt. Commun. **253**, 125 (2005).

[89] Y. Wu, W. Liu, J. Geng, X. Song, X. Ye, C.-K. Duan, X. Rong, and J. F. Du, Science **364**, 878 (2019).

[90] M. Naghiloo, M. Abbasi, Y. N. Joglekar, and K. W. Murch, Nat. Phys. **15**, 1232 (2019).

[91] F. Klauck, L. Teuber, M. Ornigotti, M. Heinrich, S. Scheel, and A. Szameit, Nat. Photonics **13**, 883 (2019).

[92] W. Cao, X. Lu, X. Meng, J. Sun, H. Shen, and Y. Xiao, Phys. Rev. Lett. **124**, 030401 (2020).

[93] T. Liu, Y.-R. Zhang, Q. Ai, Z. Gong, K. Kawabata, M. Ueda, and F. Nori, Phys. Rev. Lett. **122**, 076801 (2019).